REPORT DOCUMENTATION PAGE

AFRL-SR-AR-TR-09-0194

Public reporting burden for this collection of information is estimated to average 1 hour per response, including the time for reviewing instructions, date needed, and completing end reviewing this collection of information. Send comments regarding this burden estimate or eny other espect of this burden to Dapartment of Defense, Weshington Heedquerters Services, Directorate for Information Operetions end Reports (0704-0188), 12 4302. Respondents should be aware that notwithstanding eny other provision of law, no person shell be subject to eny penelty for feiling to com, velid OMB control number. **PLEASE DO NOT RETURN YOUR FORM TO THE ABOVE ADDRESS.**

1. REPORT DATE (DD-MM-YYYY) 02-06-09	2. REPORT TYPE Final Report	3. DATES COVERED (From - To) 02/01/2005-05/31/2009

4. TITLE AND SUBTITLE
(MEANS2 THEME) DEFECTS ASSOCIATED WITH SOLIDIFICATION OF MELT-PROCESSED SUPERALLOYS FOR THE AEROSPACE INDUSTRY AND THEIR IMPACT ON HIGH-TEMPERATURE MECHANICAL PROPERTIES.

5a. CONTRACT NUMBER

5b. GRANT NUMBER
FA9550-05-1-0089

5c. PROGRAM ELEMENT NUMBER

6. AUTHOR(S)
P. Voorhees, D. Seidman, S. Davis, T. Pollock, M. Asta

5d. PROJECT NUMBER

5e. TASK NUMBER

5f. WORK UNIT NUMBER

7. PERFORMING ORGANIZATION NAME(S) AND ADDRESS(ES)

Northwestern University   2225 Campus Drive
Department of Materials   Evanston, IL 60208
Science and Engineering

8. PERFORMING ORGANIZATION REPORT NUMBER

9. SPONSORING / MONITORING AGENCY NAME(S) AND ADDRESS(ES)
AFOSR
875 N RANDOLPH ST
ARLINGTON,VA   22203
DR. JOAN FULLER/NA

10. SPONSOR/MONITOR'S ACRONYM(S)

11. SPONSOR/MONITOR'S REPORT NUMBER(S)

12. DISTRIBUTION / AVAILABILITY STATEMENT

Approved for public release

13. SUPPLEMENTARY NOTES

14. ABSTRACT

Our Materials Engineering for Affordable New Systems (MEANS) program was centered on developing an integrated computational framework for predicting the conditions under which turbine blades can be produced that are free of deleterious solidification defects. We studied the solidification process over length scales from subnanometer to millimeter and produced a theory for defect formation. Close interaction with industry was necessary to ensure the resulting computational model will be in a form that is usable in their efforts to design new alloys and processing routes. Given the broad research focus of the project the MEANS team was composed of engineers and scientists from government laboratories, industry, and universities and is diverse in its research expertise. Our accomplishments include: Accurate prediction of liquid metal densities using ab initio molecular dynamics, development of a criterion for the stability of flows in mushy zones with heat loss, measurement of permeability of mushes using three-dimensional reconstructions, and measurement of the composition of the liquid and solid phases in mushy zones.

15. SUBJECT TERMS

16. SECURITY CLASSIFICATION OF:			17. LIMITATION OF ABSTRACT	18. NUMBER OF PAGES	19a. NAME OF RESPONSIBLE PERSON
a. REPORT	b. ABSTRACT	c. THIS PAGE			19b. TELEPHONE NUMBER (include area code)

DEFECTS ASSOCIATED WITH SOLIDIFICATION OF MELT-PROCESSED SUPERALLOYS FOR THE AEROSPACE INDUSTRY
FA9550-05-1-0089

M.D. Asta, S.H. Davis*, D.N. Seidman, P.W. Voorhees
Department of Materials Science and Engineering
*Department of Engineering Science and Applied Mathematics
Northwestern University, Evanston IL

T. M. Pollock
Department of Materials Science and Engineering
University of Michigan, Ann Arbor MI

C.F. Woodward, J.E. Spowart
Air Force Research Laboratories
Dayton, OH

This Materials Engineering for Affordable New Systems (MEANS) program focused on developing an integrated computational framework for predicting the conditions under which turbine blades can be produced that are free of deleterious solidification defects. To achieve this ambitious goal we studied the solidification process over length scales from subnanometer to millimeter and produced a fundamental experimental and theoretical framework for defect prediction. The present work aimed at producing a fundamental predictive theory in the presence of these effects and testing this criterion experimentally. A criterion for the onset of channels, freckles, and freckle chains in nickel-base superalloys relevant to the aerospace industry has been developed by Davis and Voorhees. This criterion involves the Rayleigh number that measures buoyancy in the mushy layer versus the dissipative effects of heat conduction and viscous stresses, as well as a second parameter the Biot number that measures the lateral heat loss and hence the curvature of the interface. The segregation coefficients and density parameters of multicomponent superalloys were calculated using hybrid *ab-initio*/computational-thermodynamics modeling by Asta and Woodward. The permeability of dendritic arrays in superalloys has been determined using three-dimensional reconstructions of the solid-liquid mush and finite-element fluid simulations by Pollock and Spowart.

Close interaction with industry ensured that computational models were developed in a form that is usable in their efforts to design new alloys and processing routes. Given the broad research focus of the project the MEANS team was composed of engineers and scientists from government laboratories, industry, and universities and is diverse in its research expertise.

20090630408

Background

Preventing the formation of freckles and/or misoriented grains is important to the manufacturing and performance of single crystal superalloy components. These defects are the result of solute-induced convective instabilities that occur at the solid-liquid interface during directional solidification. The two most common defects observed are isolated, individual high-angle mis-oriented grains and freckle-chains. Although a number of factors have been identified as contributors to the formation of these defects, including; cooling rates, refractory alloy content and casting size and geometry, convective flow during solidification is regarded as the precursor event. As a result, the most widely used criteria for the prediction of these defects generally consider the ratio of the buoyant to frictional forces, an interaction chiefly quantified by the Rayleigh number. Such a prediction requires not only knowledge of the fluid-flow conditions in the melt but also a detailed understanding of the geometrical domain in which the melt flows. Unfortunately, a definitive understanding of fluid flow at the scale of directionally solidified dendritic structures is still lacking. This is partly due to the many factors governing flow at this level that are both dynamic and difficult to quantify. These factors, often captured in the Rayleigh parameter R_a, Eq. (1), include composition, segregation behavior, permeability, and flow channel geometry:

$$R_a = \frac{\left(\frac{\Delta\rho}{\rho_0}\right)gKL}{\alpha v} \tag{1}$$

where $\Delta\rho/\rho_0$ is the density gradient in the liquid, g is acceleration due to gravity, K is permeability, L is the height of the mushy zone or relative length scale and αv is the product of thermal diffusivity and kinematic viscosity. Alloy chemistry influences the Rayleigh number by means of its inherent effect on the density gradient, diffusivity and viscosity.

This Rayleigh number criterion is derived from a theory of two-component solidification and is successfully used in multi-component superalloys if the thermophysical constants for segregation (and hence buoyancy) and the permeability are known. These predictions are good when the mush-melt front is horizontal; when it is not, as is often the case in practice, the theory is non-predictive. When real castings are examined, it is noted that channel and hence freckles and freckle chains preferentially form near the mold surface where heat losses, interface curvature, and horizontal permeability variations are greatest. The present work was aimed at producing a fundamental predictive theory in the presence of these effects and testing this criterion experimentally

Densities of Liquid Superalloys

In directional solidification, the mass-density difference between the hot liquid near the solid-liquid interface and the cooler melt at the top and side walls of the casting, is the driving force for convection and associated formation of solidification defects. The mass-density difference thus originates from both the composition and temperature dependencies of the liquid-phase molar volume ($V(c,T)$). We have employed ab-initio molecular dynamics simulations extensively as a computational framework for aiding the development and validation of accurate models for $V(c,T)$ in Ni-based superalloys.

AIMD simulations have been performed to derive liquid-phase atomic volumes for twelve elemental, binary and ternary alloy compositions of molten Ni with Al, W, Ta, and Re additions to compute atomic volumes at temperatures of 1830 and 1750 K. Comparisons between AIMD results and direct measurements for Ni, Ni-Al, Ni-Ta, and Ni-W yield agreement at the level of 0.6–1.8%, with the calculated volumes being systematically larger than experimental volumes. Simulations were performed for ternary alloy compositions containing W, Re and Ta, from which accuracy limits were assessed for the most recently published density parameterization at alloy compositions outside the range where experimental data is presently available.

Overall our results demonstrate the high accuracy attainable with AIMD and the utility of this method for providing data where experimental results are unavailable. They form the basis for refining the development of density models for superalloy solidification. In addition, the AIMD results present a wealth of information related to the structure and dynamics of molten alloys, useful in other contexts related to the processing of superalloys. For example, the calculated tracer diffusion coefficient for W in Ni-W molten alloys was calculated by AIMD to be $2.7(2) \times 10^{-5}$ cm^2/s, in excellent agreement with a recently published value of $2.4(2) \times 10^{-5}$ cm^2/s. Further, an analysis of the structures of the simulated binary Ni-based alloys shows a pronounced tendency towards chemical short-range ordering, and a tendency towards the preferential formation of icosahedral toplogical short-range order.
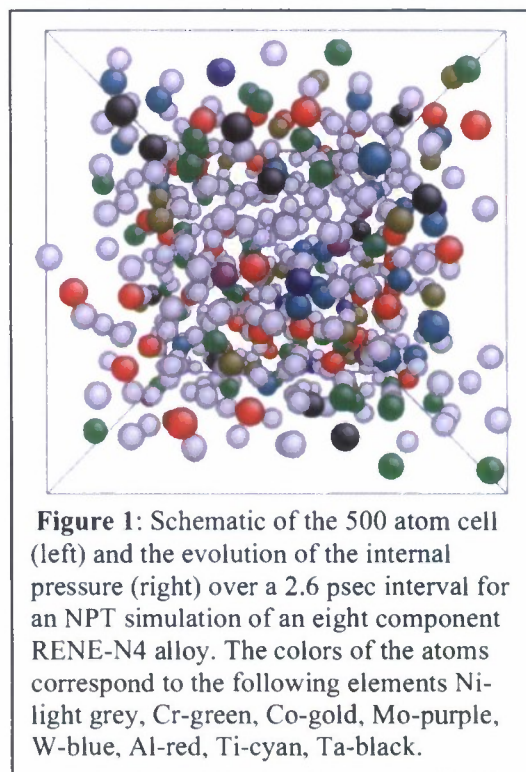

Figure 1: Schematic of the 500 atom cell (left) and the evolution of the internal pressure (right) over a 2.6 psec interval for an NPT simulation of an eight component RENE-N4 alloy. The colors of the atoms correspond to the following elements Ni-light grey, Cr-green, Co-gold, Mo-purple, W-blue, Al-red, Ti-cyan, Ta-black.

In collaboration with Jim Lill and Chris Woodward at AFRL, efforts in the latter part of this project led to the implementation constant-pressure molecular dynamics into the commercial VASP AIMD code. The new algorithms implemented in this work laid the foundation for extending the simulation methodology to real multicomponent superalloy compositions. As an example, the figure above shows a snapshot from a simulation of an eight-component model RENE-N4 superalloy which formed the focus of the experimental effort aimed at validation of Rayleigh-number criterion for the prediction of the formation of freckles and related solidification defects.

Permeability via Three-Dimensional Reconstructions

The permeability of a mush is a strong function of the morphology of the dendrites and the volume fraction of liquid. Because 3-D imaging of dendrites following complete solidification is a major challenge, our approach has been to utilize crystals where solidification has been abruptly terminated and the liquid at the solidification front is quickly decanted. Preliminary reconstructions have utilized a decanted sample of single crystal René N4 superalloy solidified in the University of Michigan Bridgman furnace. Using the prototype RoboMET3D system developed by J. Spowart and H. Mullens at Wright-Patterson Air Force Base in Dayton OH, a serial sectioning technique was developed for the René N4 alloy. Optimum slice rates of approximately 7slices/hour were reached and datasets obtained were a collection of 8-montaged images taken at 10X magnification each. The resolution of each dataset is .52um/pixel and in total the size of each dataset "slice" was on the order of 153MB. The recession rate between each imaging set was on average 2.2um. See Figure 2 for a reconstructed image.
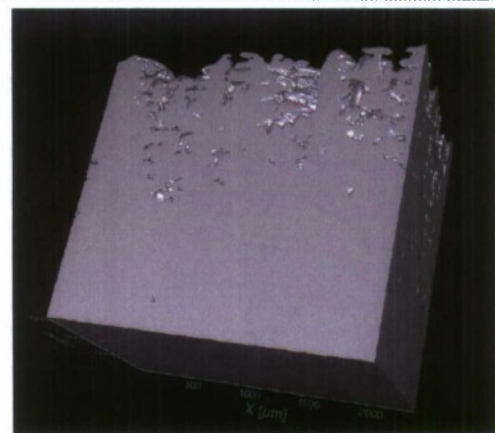

Figure 2: Reconstructed dendritic solid-liquid interface of Rene N4, gray represents solidified superalloy, the voids represent interdendritic regions occupied by liquid prior to decanting.

The three-dimensional arrays were cropped for regions of liquid connectivity and surface meshes were generated using MIMICS software by Materialise followed by volume meshes that were created in GAMBIT by ANSYS. After satisfactory meshing of the interdendritic liquid was accomplished, global smoothing of the structures was introduced to diminish the pronounced tertiary dendritic features and limit flow interaction to the primary and secondary dendrite arms to ensure convergence. FLUENT was used to simulate fluid flow through the dendritic structure in the following manner. A direction of flow was assumed and a pressure gradient is imposed on the structure. Boundary conditions of zero pressure at the outlet and a flow velocity of 100µm/sec at the inlet with 'no-slip' at the walls was assumed, and interdendritic fluid flow was assumed to be steady state. Using Darcy's Law the permeability in these structures were then calculated.

For convective instabilities to develop in a dendritic structure, flow across the dendritic array normal to the solidification direction must feed the plumes that flow parallel to the solidification direction and ultimately result in freckles. Thus the influence of dendritic structure on this "cross-flow" normal to the solidification direction is of interest. A cross-sectional volume nominally 200 x 1000 x 1500 mm was selected due to its location at the dendrite tips as well its high connectivity of interdendritic regions. Streamlines illustrating the flow directions in this volumetric cross-section are shown, Figure 3. In these simulations, flow is assumed as steady state and color bar illustrates flow speeds throughout the mushy zone. It can be observed that flow speed increases in narrow channels where flow is constricted and the flow rate must increase. Flow also seems to be dominated by the primary

4

and secondary dendrite arms found in the central portions of the region. The pertinent range of speed magnitudes observed range from 175 µm/s to 3500 µm/s. These values appear reasonable given the imposed inlet speed of 100 µm/s. We have determined the permeability of this structure to be 1.16×10^{-10} m^2.

Through this work we showed that the primary and secondary dendritic arm spacings of the reconstruction are consistent with two-dimensional measures and are within the range of expected values based upon withdrawal rates and thermal gradients. In addition, for the commercial alloy René N4, volume fraction solid as a function of height does not vary linearly with the temperature gradient as might be expected. This strongly affects the permeability as a function of depth throughout the mushy zone and particularly in the upper

Figure 3: Streamlines of cross flow through a volumetric cross-section of the mushy zone. Solidification direction is normal to the view. Velocity magnitudes are presented in m/s.

25%. Using the 3D reconstructions we find that at the solid-liquid solidification front the connectivity of the uppermost body of interdendritic liquid during solidification contains over ninety percent of the total interdendritic liquid and extends down through nearly half of the entire mushy zone height. Using these reconstructions, the permeability within these structures can be calculated based upon the observed pressure differential resulting from fluid flow. The associated permeability values calculated offer reasonable agreement with similar treatments of permeability in the literature. We find that cross-flow transverse to the primary dendrites is much more restricted that the flow parallel to the growth direction.
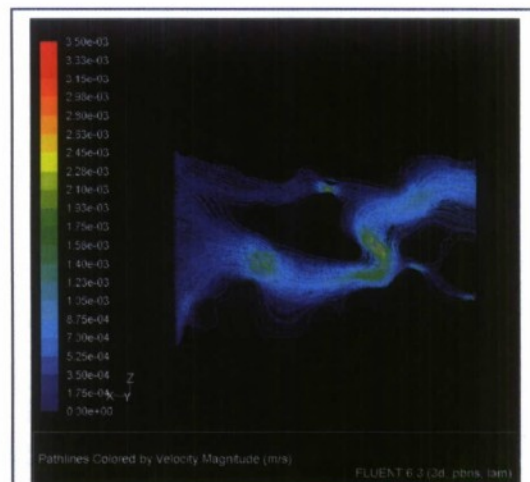
Composition of Mushes

We investigated the distribution of elements within freckles and in their surrounding matrix in Ni-based superalloys applying local-electrode atom-probe (LEAP) tomography combined with scanning and transmission electron microscopy techniques. Two directionally-solidified specimens were studied, namely ME-9 and ME-15 (S. Tin and T. M. Pollock, *Metal. Mater. Trans. A* 2003; 34A:1953). These specimens contain the elements: Ni, Al, Cr, Co, W, Mo, Ta, Re, Hf, C, and B have the nominal compositions specified by Tin and Pollock. Both alloys were investigated in their as-cast state to preserve the original partitioning of elements occurring during solidification.

Both misoriented grains and freckles were present in directionally solidified ingots. Misoriented grains are formed in the liquid close to the solidification front. Therefore, they are relatively large (on the same order of magnitude as the ingot diameter), uniformly-distributed, and have a composition similar to the average value in the solid. The mechanism of formation of freckles is, however, different. Since they are formed by thermosolutal

convection, they are smaller, aligned as chains close to an ingot's perimeter, and their composition is close to that of the last liquid remaining prior to solidification: the latter is the same as of the inter-dendritic regions of the matrix.

We determined the identity of the misoriented defects visually as well as by compositional measurements using electron energy dispersive spectroscopy (EDS). Using EDS we compared the composition of the alloy in four different regions: dendritic cores and inter-dendritic regions of both the matrix and misoriented defects (Fig. 4a). We utilized the four elements W, Re, Ta, and Mo as indicators of the partitioning behavior during solidification because it is known that Ta and Mo segregate to the liquid phase, whereas W and Re inversely-

Figure 4: The respective concentrations of W, Ta, Re, and Mo in four regions in the matrix and freckle (ME-9) measured by EDS. *(a)* Showing the partitioning behavior typical to freckles. *(b)* Showing the different partitioning behavior typical to misoriented grains (ME-15).

segregate to the solid. We observed both types of partitioning behavior. In the freckles, similar compositions were measured in regions B, C, and D, which are different from that of region A (Fig. 4b). The average composition of the misoriented grains was, however, about the same as that of the matrix (Fig. 4c). In both cases, the concentrations of W and Re are larger in the dendritic cores than in the inter-dendritic region, whereas Ta and Mo exhibit the opposite trend.
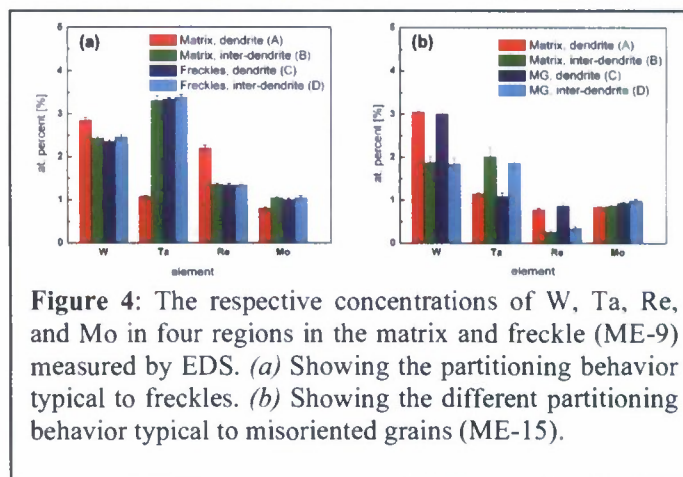
The microstructure of both alloys is not homogeneous at all pertinent length scales. Therefore, we decided to reconsider the previously-proposed methodology of sample preparation for LEAP tomography, which was cutting an array of tips from a freckle and its immediate vicinity. It is, however, valuable to employ the conventional method (cutting thin rods and electrochemically sharpening) for precise measurements of the average composition in large misoriented grains. Both the matrix and a misoriented grain for alloy ME-9 were analyzed; however, results were collected only for the $\gamma\gamma$'-phase since it occupies the majority of the volume. Only one tip exhibited a mixture of both the γ-γ and $\gamma\gamma$'-phases, from which we draw a conclusion about the average composition of the grain. The phases can be determined from the different partitioning behavior of the elements. Fig. 5 is an example of a 3-D reconstruction, showing the distribution of three atomic species, for the sake of clarity: Al (red dots), Cr (blue dots), and C (spheres). The interface between the γ-γ and $\gamma\gamma$'-phase was determined using a 9.3 at.% Cr
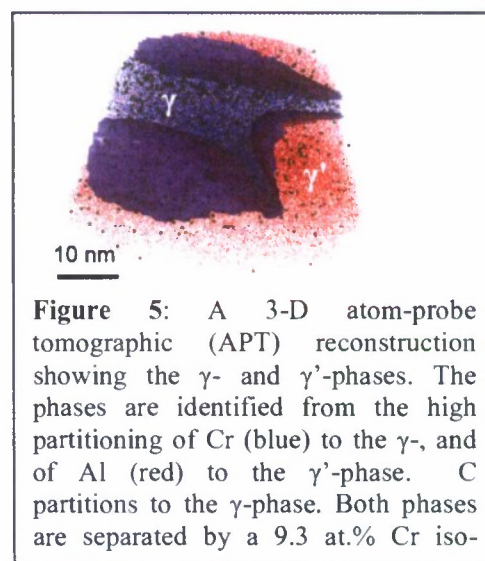

Figure 5: A 3-D atom-probe tomographic (APT) reconstruction showing the γ- and γ'-phases. The phases are identified from the high partitioning of Cr (blue) to the γ-, and of Al (red) to the γ'-phase. C partitions to the γ-phase. Both phases are separated by a 9.3 at.% Cr iso-

6

isoconcentration surface. The other elements (not presented herein) exhibit different partitioning behaviors: Cr, Co, W, Re, Mo, Hf, B, and C partition to the γ-phase, while Ni, Al, and Ta - to the γ'-phase. The partitioning ratios of each of the elements were also determined. Although this trend is general, there are some exceptions in which the partitioning behavior of minority elements is reversed. For example, we find the (slight) preference of W for the γ-phase is reversed in favor of the γ'-phase as a result of the presence of Ta. We hypothesized that because of tantalum's preference for the Al-sublattice sites of the γ'-phase, Ta has a stronger tendency to occupy these sites, thus rejecting the W atoms to the γ-phase. We confirmed this hypothesis employing first-principles calculations, using VASP, of the substitutional formation energies of W and Ta at different sites in both the γ- and γ'-phases. The calculations demonstrated that the energetic driving force for Ta partitioning to the γ'- phase is twice that of W.

The additional method we utilized to investigate the composition in the four regions of interest (see Fig. 4) involves lifting-out samples from these regions using a FEI Helios dual-beam focused-ion beam (FIB) microscope (FIB). This procedure is illustrated in Fig.6.

In this framework, we developed a method that enables us to take advantage of the superior detectability and mass resolution of the LEAP tomograph, and the ability to quantify elemental concentrations at much longer length scales (10-100 μm) than those typically obtained using atom-probe tomography (10-100 nm).
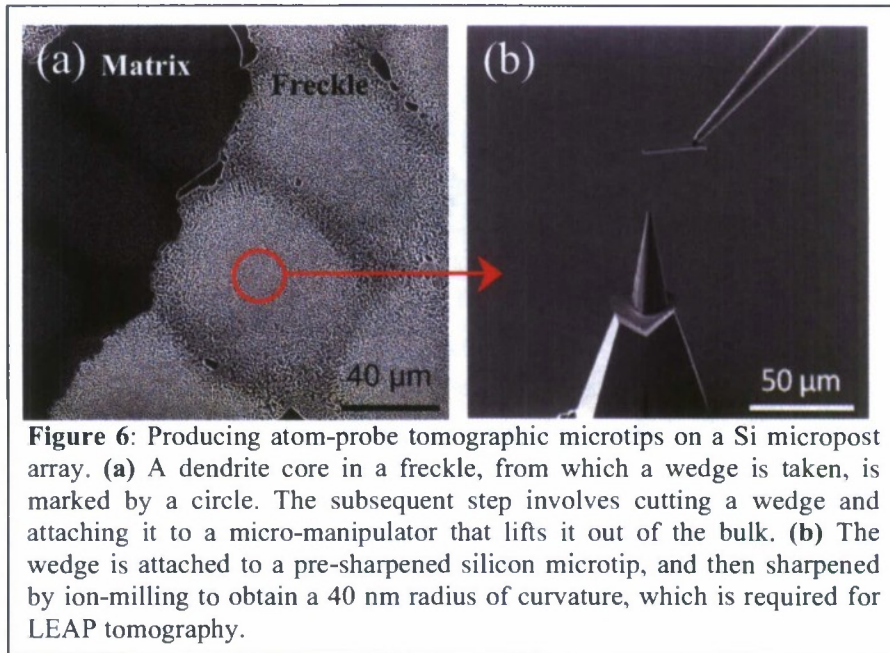

Figure 6: Producing atom-probe tomographic microtips on a Si micropost array. (a) A dendrite core in a freckle, from which a wedge is taken, is marked by a circle. The subsequent step involves cutting a wedge and attaching it to a micro-manipulator that lifts it out of the bulk. (b) The wedge is attached to a pre-sharpened silicon microtip, and then sharpened by ion-milling to obtain a 40 nm radius of curvature, which is required for LEAP tomography.

Our technique is based on a mass balance existing between the γ- and γ'-phases (Eq.1), and is applicable for all LEAP 3-D reconstructions comprising both the γ- and γ'-phases, Fig. 5. The difference between the average concentration of an element i in the dendrite cores (C_{avg} - measured by EDS) and its concentration in the γ-phase alone (C_γ, measured by APT) is plotted against the difference between the content of i in γ'($C_{\gamma'}$) and γ, respectively.

$$C_{avg} = C_\gamma + \left(C_{\gamma'} - C_\gamma\right)\phi_{\gamma'} \qquad (1)$$

This procedure is made for all elements detected employing EDS. The result is a linear dependence with a slope equals to the volume fraction of γ'($\phi_{\gamma'}$). A very useful application of this scheme, besides indicating the consistency between EDS and APT, is that, in this manner, we can derive the *average* composition of *any* element in the dendrite core (or any of the other 4 regions of interest), even for those not detected by EDS: see results in Fig. 7.

Based on the above methodology, we estimated the solid/liquid partitioning behavior of Hf. In contrast with other elements (such as W, Re, Ta, Mo), of which the partitioning behavior (and, therefore, their role in freckle formation) is known, there are insufficient data regarding the solid/liquid partitioning behavior of Hf, since the Hf content is usually too small to be quantified by conventional means, such as EDS. Although the nominal Hf concentration is relatively low (0.05 at.%), the question of Hf micro-segregation to the solid/liquid interface during solidification is important, since it is a heavy element (178.49 g mole⁻¹) and is, therefore, more likely to cause density inversion that results in thermosolutal convection and freckle formation. The result is an average concentration of Hf in the *matrix* dendrite cores of 0.10±0.01 at. % and 0.148±0.012 at. % for the ME-9 and ME-15 alloys, respectively. These values are much larger than the nominal Hf concentration of both samples, 0.05 at.%, indicating that Hf partitions to the dendrite cores (solid). Moreover, no Hf was detected in the samples lifted-out from the *freckles* dendrite cores. We

Figure 7: A mass-balance diagram plotted for the matrix dendrite cores in the ME-9 alloy. The elements shown are detected by EDS, while the concentration of the other minority elements can be interpolated using the fitting formula.

conclude that Hf, by partitioning to the solid during solidification, reduces the average density in the liquid and this may enhance freckle formation. Quantitatively, we evaluated the liquid density using a semi-empirical expression for the density of a multi-component liquid (P. K. Sung, D. R. Poirier, and E. McBride, *Mater. Sci. Eng. A* **231** (1-2):189, 1997), which takes into account a mixing term, ΔV^M, Eq.(2):

$$\rho = \sum_i x_i M_i / \left[\sum_i x_i M_i / \rho_i + \Delta V^M \right]$$ (2)

The liquid density decreases by 0.12% due to Hf depletion, whereas observations (R.A. Hobbs, S. Tin, C.M.F. Rae, *Metall. Mater. Trans.* **36A**: 2761, 2005) indicate that freckles appear only when the density inversion term exceeds 2-5%.

Using the above techniques we quantified the compositions in the dendrite cores of the matrix and freckles of the ME-15 alloy using LEAP tomography. The other regions (inter-dendritic), were analyzed only using EDS. Based on Eq.(2), we estimated the density inversion term, ($\Delta\rho/\rho_o$), to be 2% and 0.5% in the Me-15 and ME-9 alloys, respectively.
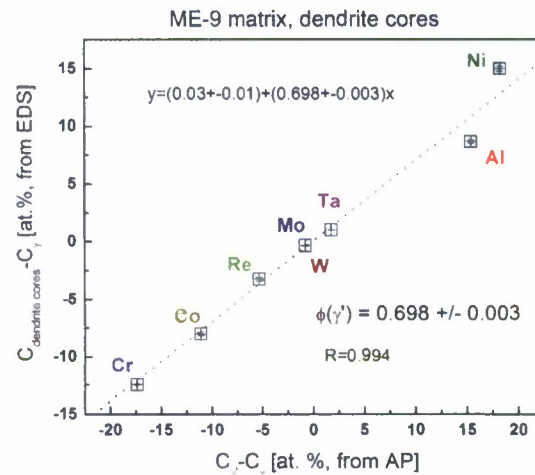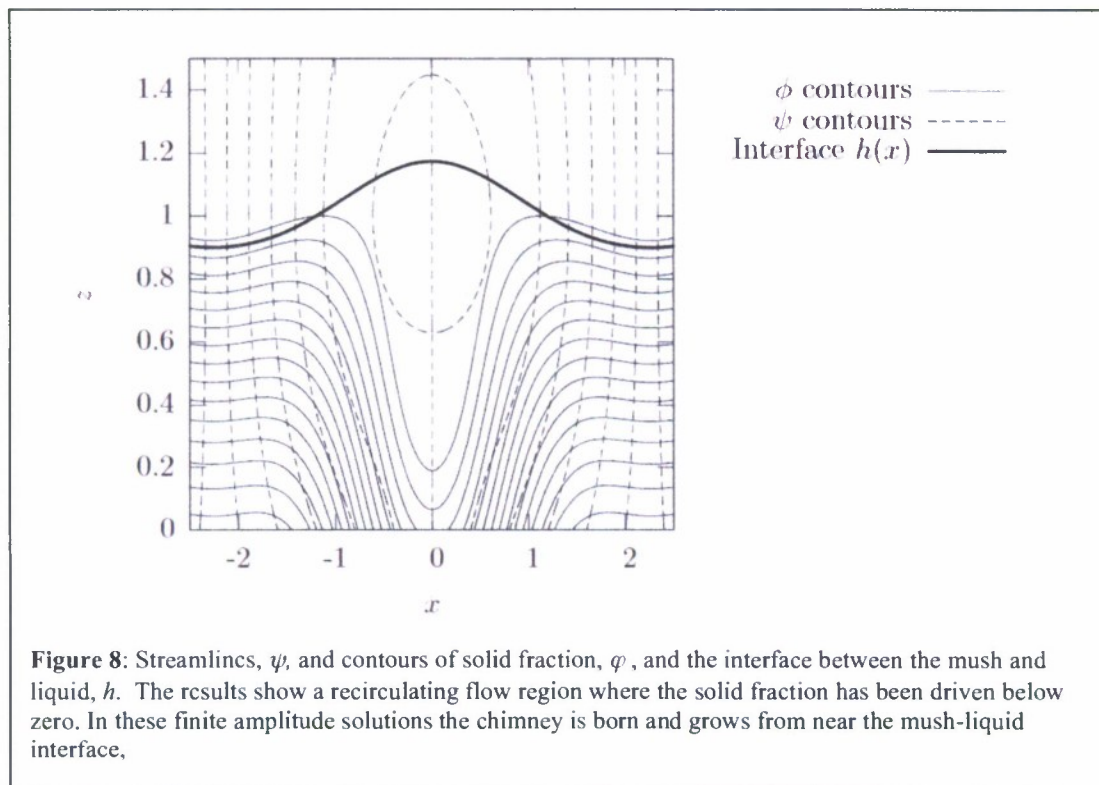
8

Theory of Flow in Mushy Zones

We examined the convective state due to weak sidewall heat losses in a mushy zone during the steady directional solidification of a binary alloy. The configuration consisted of a warm liquid region and a cold solid region separated by a mixed phase region, the mushy zone, which is modeled as a reactive porous matrix. The structure of the convection that arises from horizontal temperature gradients, induced by the heat losses at the sidewalls, is characterized by a set of nondimensional parameters that describe the effects of latent heat, composition, permeability, and thermal and solutal buoyancy. We observed a wide range of behaviors and showed that, as the critical Rayleigh number for convection in a horizontally uniform mush is reached, we begin to see the precursors of chimneys near the cooled boundaries. The strength of the cooling plays an important role in determining the strength and degree of localization of the convection near the boundary. We find, in common with other authors, that upflow, in this case caused by lighter fluid being released at the cooled sidewalls, leads to regions of dissolution, which are precursors to chimney formation. We also indentified the effects of the different physical parameters on the steady states convection patterns.

The above mentioned stability theory shows that, indeed, nonlinear instabilities grow preferentially near the walls, where the up flow melts away the dendritic structure producing channels. The conditions for chimney growth depend not only on the local Rayleigh Number the measures buoyancy, but the Biot Number that measure the heat losses.

Most importantly, this paper showed why a correlation depending on Rayleigh Number only reasonably predicts the conditions of chimney growth when the front is flat, but fails when it is curved (here, by heat losses). The proper criterion depends both on Rayleigh Number and a second parameter that measures front curvature and hence horizontal convection.

We also examined the dynamics of a mushy layer in directional solidification for the case of a thin, near-eutectic mush with a deformable and permeable mush-liquid interface. We focused on the onset of convection using linear stability analysis, and the weakly nonlinear growth of liquid inclusions that signal the onset of chimneys. This analysis was compared to past analyses in which the mush-liquid interface is replaced by a rigid, impermeable lid. We found qualitative agreement between the two models but the rigid-lid approximation gave substantially different quantitative behavior. In linear theory the rigid-lid approximation leads to an over-estimate of the critical Rayleigh number and wave number of the instability by as much as a factor of about 5 and 2 respectively. The onset of oscillatory instability was also changed by a factor of about 5 in composition number C. In the weakly-nonlinear theory, the location of the onset of liquid inclusions is near the undisturbed front for the free-boundary analysis whereas it lies at the centre of the mushy layer when the rigid-lid approximation is used. An example of the onset of chimneys that follow from this calculation is given in Figure 8.

Figure 8: Streamlines, ψ, and contours of solid fraction, φ, and the interface between the mush and liquid, h. The results show a recirculating flow region where the solid fraction has been driven below zero. In these finite amplitude solutions the chimney is born and grows from near the mush-liquid interface,

Personnel Supported

M. Asta	Professor, University California Davis
D. Trinkle	Postdoc, Air Force Research Laboratory and Professor UIUC
D. Seidman	Professor, Northwestern University
Y. Amouyal	Postdoc, Northwestern University
P. Voorhees	Professor, Northwestern University
R. Mendoza	Postdoc, Northwestern University
T. Pollock	Professor, University of Michigan
J. Madison	Graduate Student, University of Michigan
S. Davis	Professor, Northwestern University
S. Roper	Postdoc, Northwestern University

Publications

M. Asta, D. Trinkle and C. Woodward, "Ab-Initio Molecular Dynamics Simulations of Molten Ni-Based Superalloys," to be published in the IEEE proceedings of the DoD High Performance Computing Modernization Program 2006 Users Group Conference.

J. Madison, J.E. Spowart, D.J. Rowenhorst, J.Fiedler, T.M. Pollock, *Characterization of Three Dimensional Dendritic Structures in Nickel-Base Single Crystals for Investigation of Defect Formation*, Superalloys 2008, TMS Warrendale, PA, (2008).

J. Madison, J.E. Spowart, D.J. Rowenhorst and, T.M. Pollock, "*Three Dimensional Reconstruction of the Dendritic Structure at the Solid-Liquid Interface in a Ni-Base Single Crystal*", JOM, July 2008, *in press.*

J. Madison, J. Spowart, K. Thornton and T.M. Pollock "*Permeability of Directionally Solidified Dendritic Structures in a Ni-Base Superalloy*", Acta Materialia, in preparation.

J. Madison, M. Asta, P. Voorhees and T.M. Polloek, "*Convective Instabilities in a Ternary Ni-Al-W Single Crystal*", Aeta Materialia, in preparation.

S.M. Roper, S.H. Davis, and P.W. Voorhees, *An Analysis of Convection in a Mushy Layer with a Deformable Permeable Interface,* J. Fluid Meeh. **596** 333-352 (2008).

S.M. Roper, S.H. Davis and P.W. Voorhees, *Convection in a Mushy Zone Forced by Sidewall Heat Losses*, Metall. Trans. A, 38A 1069-1079 (2007).

Yaron Amouyal, Zugang Mao, David N. Seidman, *Segregation of tungsten at $\gamma'(L1_2)/\gamma(f.c.c.)$ interfaces in a Ni-based superalloy: An atom-probe tomographic and first-principles study*, Appl. Phys. Lett. 93 (20), 201905 (2008).

Yaron Amouyal, Zugang Mao, Christopher Booth-Morrison, David N. Seidman, *On the interplay between tungsten and tantalum atoms in Ni-based superalloys: An atom-probe tomographic and first-principles study.* Appl. Phys. Lett. 94 (4), 041917 (2009).